# Influence of Si addition on the carbon partitioning process in martensitic-austenitic stainless steels

**Q Huang[1], O Volkova[1], BC De Cooman[2], H Biermann[3] and J Mola[1,*]**

[1] Institute of Iron and Steel Technology, Technische Universität Bergakademie Freiberg, Leipziger Str. 34, 09599, Freiberg
[2] Graduate Institute of Ferrous Technology, Pohang University of Science and Technology, Pohang, Gyeongbuk 790-784, South Korea
[3] Institute of Materials Engineering, Technische Universität Bergakademie Freiberg, Gustav-Zeuner-Straße 5, 09599 Freiberg, Germany

[*] e-mail: mola@iest.tu-freiberg.de

**Abstract.** The effect of Si on the efficiency of carbon partitioning during quenching and partitioning (Q&P) processing of stainless steels was studied. For this purpose, 2 mass-% Si was added to a Fe-13Cr-0.47C reference steel. The Si-free (reference) and Si-added steels were subjected to Q&P cycles in dilatometer. The carbon enrichment of austenite in both steels was evaluated by determining the temperature interval between the quench temperature and the martensite start temperature of secondary martensite formed during final cooling to room temperature. In Q&P cycles with comparable martensite fractions at the quench temperature, the carbon enrichment of austenite after partitioning was similar for both steels. To compare the mechanical stability of austenite, Q&P-processed specimens of both steels were tensile tested in the temperature range 20-200 °C. The quench and partitioning temperatures were room temperature and 450 °C, respectively. Si addition had no meaningful influence on mechanical stability of austenite. The results indicate that the suppression of cementite formation by Si addition to stainless steels, as confirmed by transmission electron microscopy examinations, has no noticeable influence on the carbon enrichment of austenite in the partitioning step.

## 1. Introduction

Introduction of retained austenite (RA) in the microstructure of martensitic steels has been one of the focuses in recent advanced high strength steel developments, with the aim to enhance the ductility of steels without severe sacrifice of the strength. This objective may be achieved by appropriate alloy and processing design. Due to its simplicity and efficiency in stabilizing austenite, a thermal processing method known as quenching and partitioning (Q&P) processing has received especial attention [1–5]. This heat treatment consists of quenching austenite to a temperature between martensite start ($M_s$) and finish ($M_f$) temperatures, followed by a partitioning treatment at higher temperatures to allow the diffusion of carbon from martensite to austenite, therefore stabilizing austenite at room temperature (RT) [6].

As the precipitation of carbides competes with the carbon enrichment of austenite, Q&P steels are usually alloyed with Si [7–9]. Si is known to suppress the formation of cementite, presumably due to its extremely low solubility in cementite [10]. Dilatometry experiments have indicated that the onset of cementite during continuous heating of low-alloy steels with 0.7 mass-% C is raised by

approximately 200 °C by the addition of 2 mass-% Si [10]. Nevertheless, evidences of cementite formation in low-alloy martensitic steels containing up to 2 mass-% Si have been presented after tempering at relatively high temperatures [11,12]. In theory, if carbide precipitation is inhibited, more carbon is available for partitioning into RA. Accordingly, Si addition has been reported to increase the final RA fractions [13] or raise the carbon concentration of Q&P-processed carbon and low-alloy steels [14,15]. As an example, carbon partitioning between martensite and austenite was negligible in the Fe-1.1C-3Mn steel (concentrations in mass-%) partitioned at 300 °C, but it was noticeable in the steel containing 2 mass-% Si after applying the same Q&P routine [16].
The enhanced carbon enrichment of partitioned austenite upon Si addition occurs mostly during the formation of carbide-free bainite [17–19]. The latter is a result of isothermal decomposition of austenite in the partitioning step of carbon and low-alloy steels and is a common problem encountered during the Q&P processing of such steels [20–22]. In the case of stainless steels, on the other hand, the transformation of RA into bainite is inhibited by the presence of high Cr contents [23] which makes them ideal candidates for the Q&P processing. Nevertheless, the presence of high Cr contents is not effective against the formation of $M_3C$ cementite (M denotes Fe and substitutional elements) [24]. The precipitation of cementite in martensitic stainless steels can be retarded by the addition of Si [25]. Accordingly, Si addition to stainless steels is expected to enhance the carbon partitioning efficiency. Tobata *et al.* reported an increase in the fraction of RA in Q&P-processed martensitic stainless steels upon the addition of Si which was ascribed to the reduced $M_3C$ formation [26]. Nevertheless, although carbon concentration in the partitioned austenite was not given, the variation of austenite lattice parameter during partitioning was similar for the Si-free and Si-added steels.
The lack of convincing experimental proof for the theoretical expectation of enhanced carbon enrichment of austenite in the absence of $M_3C$ precipitates casts doubt on the efficiency of Si on the Q&P response of steels. The present study aims at clarifying the role of Si in the Q&P processing of stainless steels. For this purpose, Si-added and Si-free steels were subjected to Q&P cycles in dilatometry to evaluate the carbon enrichment of RA. Furthermore, the mechanical stability of austenite was compared by tensile testing of Q&P steels at temperatures ranging from RT to 200 °C.

## 2. Experimental procedure

Steels with the chemical compositions shown in Table 1 were produced in a vacuum induction and casting facility. The Si-free and Si-added steels are denoted as Cr and CrSi steels, respectively. The cast ingots were forged and caliber rolled to round bars with a diameter of 12 mm. A Bähr 805 pushrod dilatometer was used to simulate the Q&P cycles shown in Figure 1(a). Since the partitioning of carbon is more pronounced in the presence of martensite fractions above approximately 50 vol.% [27], the solution annealing temperature was 1050 °C where Cr-rich carbides are only partially in solution [28].The application of a high cooling rate of 20 °C/s between annealing temperature and 500 °C intended to prevent the growth of Cr-rich carbides upon cooling. Below 500 °C, cooling rate was reduced to 3 °C/s. The possibility of applying high quench temperatures enables to track changes in the secondary $M_s$ temperature without the need for subzero dilatometry. Quench temperature (QT) in dilatometry cycles was varied between 170 °C and 200 °C and the partitioning was done at 450 °C for 3 min.
In order to compare the carbon contents of austenite in both steels at 1050 °C, $M_s$ temperatures after annealing at 1180 °C and 1050 °C were determined by dilatometry. At 1180 °C, Cr-rich carbides are fully dissolved in the austenitic matrix [28]. Therefore, carbon concentrations of austenite at 1180 °C are equal to the nominal values in both steels. Considering that the addition of each 1 mass-% solute carbon in austenite reduces the $M_s$ temperature of stainless steels by approximately 510 °C [23], the carbon concentrations of austenite at 1050 °C can be estimated based on the rise in $M_s$ temperature caused by decreasing the annealing temperature from 1180 °C to 1050 °C.
The mechanical stability of RA in Q&P steels was evaluated by tensile tests. In order to enhance the stability of RA in comparison with dilatometry cycles, the carbon loss of austenite due to undissolved Cr-rich carbides was avoided by solution annealing at 1250 °C. According to [28], this temperature is sufficiently higher than the full dissolution temperature of Cr-rich carbides in the Si-free steel (1125 °C). As shown in Figure 1(b), the Q&P processing was simplified as the QT was equal to RT.

Quenching was done with He to achieve an average cooling rate of approximately 30 °C/s between 1250 °C and 400 °C. The cooling rate was lower at temperatures near RT. Subsequently, the specimens were partitioned at 450 °C for 5 min and air cooled to RT. Tensile tests were carried out in a Zwick/Roell-UPM 1476 type universal testing machine. The crosshead displacement speed was kept constant at 1.8 mm $min^{-1}$, corresponding to an initial strain rate of approximately $8 \times 10^{-4}$ $s^{-1}$. Tensile specimens with a diameter of 6 mm and a parallel length of 36 mm were machined according to the DIN 50125 standard. At least two tensile specimens from each steel were tested at each temperature. Furthermore, in order to evaluate the solid solution strengthening effect of Si, two Q&P tensile specimens of each steel were annealed at 700 °C for 5 h and then tensile tested at RT.
The martensite fraction of dilatometry specimens quenched directly from 1050 °C to RT and those of the tensile specimens before and after straining were measured by magnetic saturation measurements using a Metis MSAT device equipped with a Lakeshore 480 fluxmeter. As the only ferromagnetic phase in the microstructure, the fraction of martensite can be quantified by dividing the measured mass magnetization by the intrinsic mass magnetization of the martensitic constituent. The martensite fractions at different stages of dilatometry Q&P cycles were calculated based on the associated expansions. For this purpose, use was made of the lever rule in a manner similar to that described in [24]. The correlation between the magnitude of expansion and the fraction of martensite was established by quantifying the martensite fraction of dilatometry specimens by magnetic measurements. Transmission electron microscopy (TEM) examinations were done in a JEOL JEM-2100 type TEM with a $LaB_6$ gun operated at 200 kV. TEM samples were prepared by mechanical polishing to a thickness of approximately 100 μm followed by twin-jet polishing at RT with an electrolyte of 5 % perchloric acid in 95 % acetic acid.

**Table 1.** Chemical compositions of the studied steels in mass-%

| Steel ID | C | Cr | Si | Mn | N | Fe + others |
|---|---|---|---|---|---|---|
| **Cr** | 0.473 | 13.1 | 0.377 | 0.359 | 0.008 | Bal. |
| **CrSi** | 0.466 | 12.8 | 2.050 | 0.353 | 0.010 | Bal. |

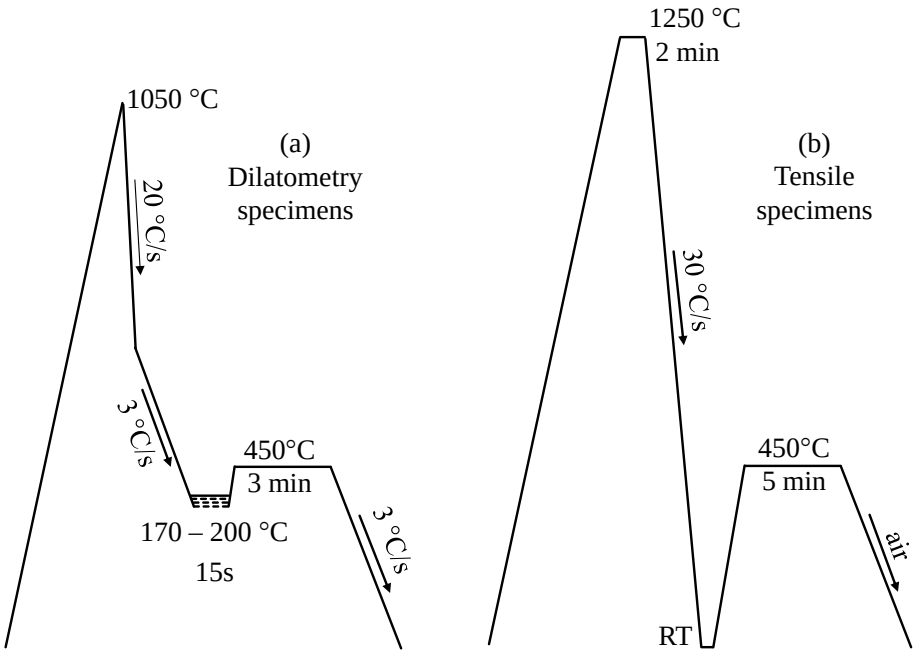


**Figure 1.** Schematic illustration of Q&P processing for (a) dilatometry specimens and (b) tensile specimens.

## 3. Results and discussion

Figure 2 shows the relative length changes during quenching of the steels from 1050 °C and 1180 °C. Relative length changes during quenching from 1050 °C are exemplified by two Q&P cycles with the routines shown in Figure 1(a). The QTs are 170 °C and 200 °C for the Cr and CrSi steels, respectively. After quenching from 1180 °C, due to the full dissolution of Cr-rich carbides at 1180 °C [28] , carbon concentrations of austenite and martensite are equal to the nominal values in both steels. The $M_s$ temperatures for the Cr and CrSi steels after annealing at 1180 °C were 124 °C and 98 °C, respectively. Due to the presence of undissolved Cr-rich carbides, the $M_s$ temperatures are higher for the annealing temperature of 1050 °C, namely they are 260 °C and 239 °C for the Cr and CrSi steels, respectively. As an increase of 1 mass-% solute carbon in austenite depresses the $M_s$ temperature of stainless steels by nearly 510 °C [23], the drops of 136 °C and 141 °C in the $M_s$ temperature can be correlated with reductions of 0.267 and 0.276 mass-% in the solute carbon content of Cr and CrSi steels, respectively. The comparable carbon losses of austenite upon the formation of Cr carbides implies that the solute carbon contents of austenite in the Cr and CrSi steels remain comparable after solution annealing at 1050 °C, which was also used as the annealing temperature for the dilatometry experiments represented in Figure 1(a).

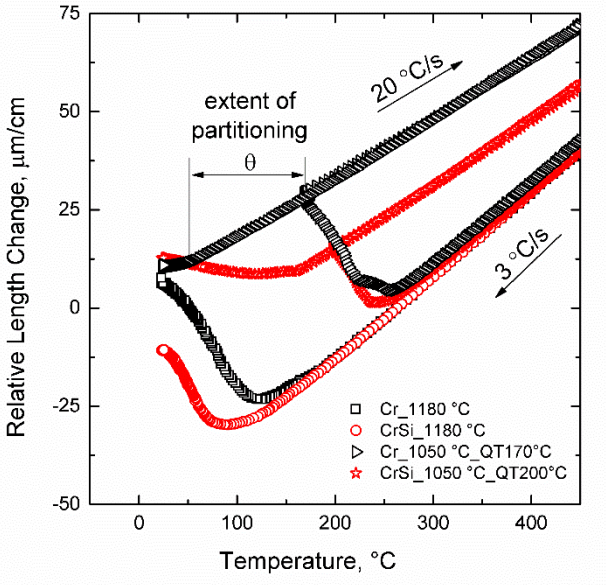


**Figure 2**. Relative length changes during cooling of Cr and CrSi steels from 1050 °C and 1180 °C. Cooling from 1050 °C was interrupted at 170 °C for the Cr steel and at 200 °C for the CrSi steel. Subsequent to interruption, specimens were reheated to 450 °C, held for 3 min, and finally cooled to RT at 3 °C/s.

The stabilization of RA during Q&P processing originates from its carbon enrichment during partitioning. As a result, the austenite cooled from the partitioning temperature transforms to secondary martensite at a temperature lower than the applied QT. In the present study, the temperature interval (θ) between QT and secondary $M_s$ temperature (marked in Figure 2) was used to quantify the extent of partitioning. To exclude the effect of Si addition on the $M_s$ temperature, θ is plotted against the primary martensite fraction ($f_{a'}$), namely the fraction of martensite present before partitioning. Presence of identical primary martensite fractions ensures that the amount of carbon available for partitioning into the austenite remains comparable. The results of dilatometry Q&P cycles according to Figure 1(a) are summarized in Figure 3. The secondary $M_s$ temperature for the CrSi steel quenched to 170 °C was below RT. Therefore, the associated θ could not be determined by dilatometry and is not given in Figure 3. As shown in Figure 3(a), the primary $f_{a'}$ at an identical QT is higher for the CrSi steel than it is for the Cr steel. At first glance, this might appear inconsistent since the martensitic expansions for both alloys are very similar in the vicinity of 200 °C (Figure 2). Nevertheless, the expansion caused by martensite formation is somewhat smaller for the CrSi steel than that for the Cr steel. According to correlative dilatometry and magnetic saturation measurements, the formation of each vol.% martensite in the Cr steel is associated with an expansion of nearly 0.0094 % at RT. For the CrSi steel, this value is reduced to 0.0076 % indicating that the CrSi steel undergoes a smaller

expansion upon the formation of martensite. This result agrees with the dilatometry expansions for low-alloy steels with and without Si [10] and can be related to the lattice contraction of bcc steels upon alloying with Si [29].

For the primary $f_{a'}$ of nearly 44 vol.%, θ in the Cr steel is higher than that for the CrSi steel. The difference in θ values for the Cr and CrSi steels is much smaller when primary $f_{a'}$ exceeds 50 vol.%. The maximum difference in θ of 18 °C, observed in the presence of approximately 44 vol.% martensite, corresponds to a difference in the carbon enrichment of only 0.035 mass-%. In accordance with the θ values, the difference in the secondary $f_{a'}$ formed in the presence of a given primary $f_{a'}$ is negligible for both steels. The results indicate that, in contrast to the common belief, the carbon enrichment of austenite during Q&P processing of stainless steels is not much influenced by the addition of Si.

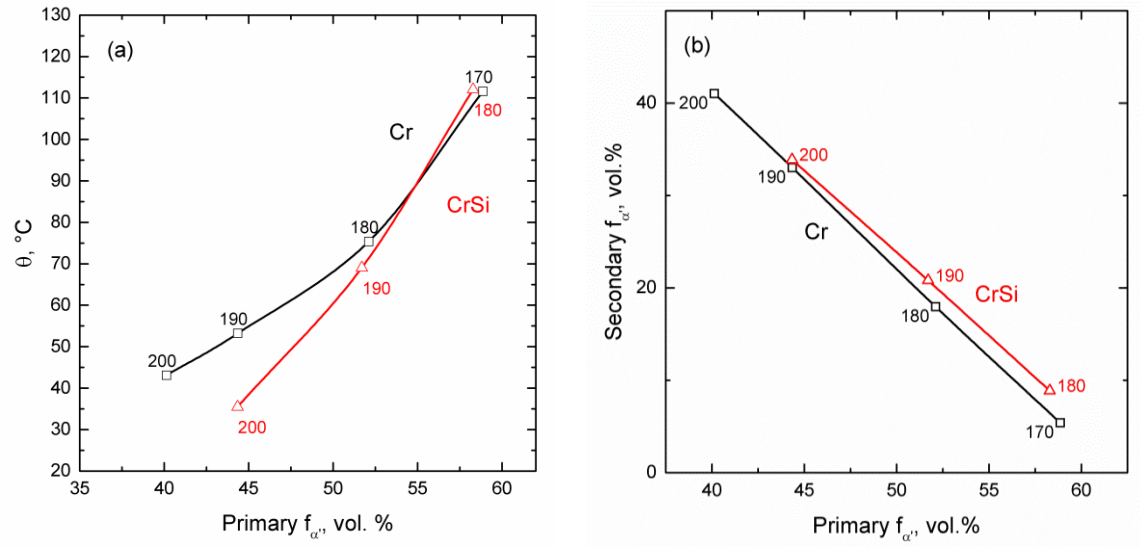


**Figure 3.** Variation of stabilization parameter θ (a) and secondary martensite fraction (b) with the primary martensite fraction. The numbers next to symbols denote the respective quench temperatures.

TEM investigations of the Cr steel quenched in liquid nitrogen from the solution annealing temperature of 1250 °C and tempered at 400 °C revealed the existence of $M_3C$-type carbides in the martensitic constituent (Figure 4(a)). As shown in Figure 4(b), such carbides do not form in the martensite phase of the CrSi steel heat treated in the same manner. The observation of similar degrees of stabilization for the austenite in the Cr and CrSi steels (dilatometry results) indicates that the suppression of $M_3C$ formation in the martensite does not promote the extent of carbon partitioning into the RA. Therefore, either more carbon remains as solute in the martensite phase of the CrSi steel or alternative carbon-consuming processes such as segregation to defects proceed to a larger extent for the CrSi steel.

The mechanical stability of RA in the steels treated by the simplified Q&P processing as shown in Figure 1(b) was determined by tensile testing at various temperatures. According to magnetic saturation measurements, the martensite fractions prior to tensile tests were 44 vol.% and 43 vol.% for the Cr and CrSi steels, respectively. The engineering stress-engineering strain curves are shown in Figures 5(a and b). In the studied temperature range, the CrSi steel shows both higher tensile strengths and higher tensile elongations. The temperature dependence of tensile elongation is summarized in Figure 5(c). Both steels exhibit poor ductility at RT and 80 °C. As the temperature increases, the tensile elongation increases in both steels which is due to the enhanced austenite stability and its delayed deformation-induced transformation to martensite [30,31]. The mechanical stability of austenite was quantified using the following equation as proposed by Sugimoto et. al. [32]:

$$k = -\ln((f_\gamma^0 - f_{\alpha'}^d) \cdot (f_\gamma^0)^{-1}) \cdot \varepsilon^{-1} \quad (1)$$

where $k$ is a parameter inversely proportional to the stability of austenite, $f_\gamma^\circ$ is the initial austenite fraction, $\varepsilon$ is the applied true strain in tension, and $f_\alpha^d$ is the deformation-induced martensite fraction after applying the true strain $\varepsilon$. $f_\gamma^\circ$ was calculated from the martensite fraction in the grip section by assuming a carbide fraction equal to zero. The difference in the martensite fraction between the grip and gauge sections was taken as $f_\alpha^d$, which is given in Figure 6(b). The local true strains shown in Figure 6(a) were obtained based on the reduction in area of nearly cylindrical specimens taken from the gauge sections of tensile-tested specimens. The calculated $k$ parameters are plotted in Figure 6(c) as a function of the tensile test temperature. At 20 °C and 80 °C, the CrSi steel exhibits somewhat smaller $k$ values, indicative of higher mechanical stabilities compared to the Cr steel. The difference in $k$ values becomes negligible at 160 °C and 200 °C. Due to the higher area reductions at these temperatures and the higher certainty of local strain readings based on the diameter change measurements, the $k$ values at 160 °C and 200 °C are expected to be better representatives of the mechanical stability of austenite. The negligible difference between the mechanical stability of austenite in the Cr and CrSi steels is in accordance with the dilatometry observations suggesting the inefficiency of Si addition in increasing the stability of austenite. Therefore, the importance of cementite suppression by Si addition on the efficiency of carbon partitioning might have been overestimated.

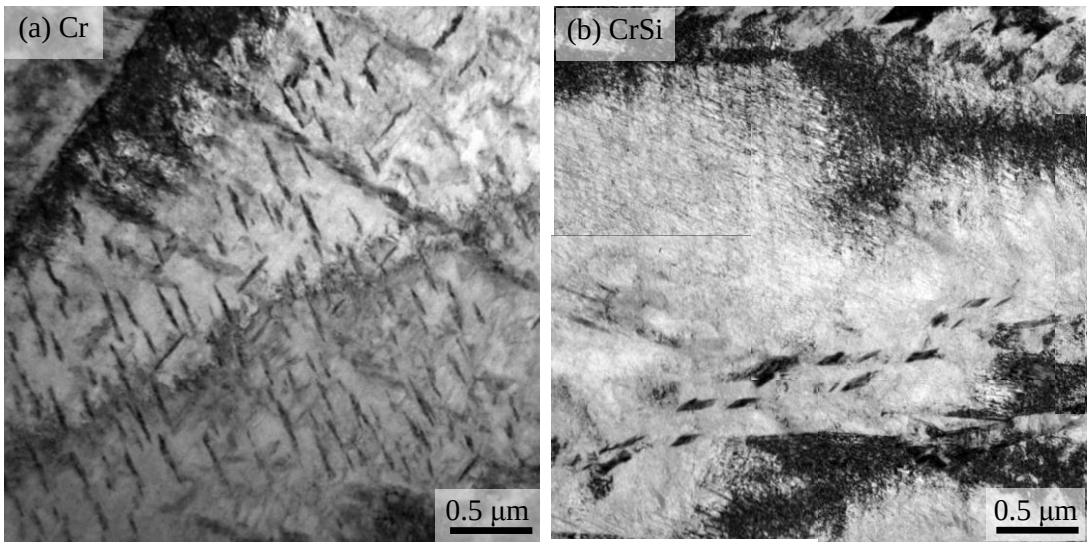


**Figure 4.** TEM bright-field micrographs of (a) Cr steel and (b) CrSi steel partitioned at 400 °C for 5 min subsequent to quenching from 1250 °C to -196 °C.

The higher strength of the CrSi steel in spite of having a martensite fraction comparable to that of the Cr steel was speculated to be related to the solid solution strengthening effect of Si. In order to verify this, tensile specimens Q&P processed according to Figure 1(b) were soft annealed at 700 °C for 5 h to obtain a low carbon ferritic matrix containing dispersed $M_{23}C_6$ carbides. The soft-annealed steels were then tensile tested at RT (Figure 7). The obviously higher tensile strength of the CrSi steel confirms that the higher strength of the Q&P tensile specimens of the CrSi steel may be attributed to the solid solution strengthening effect of Si.

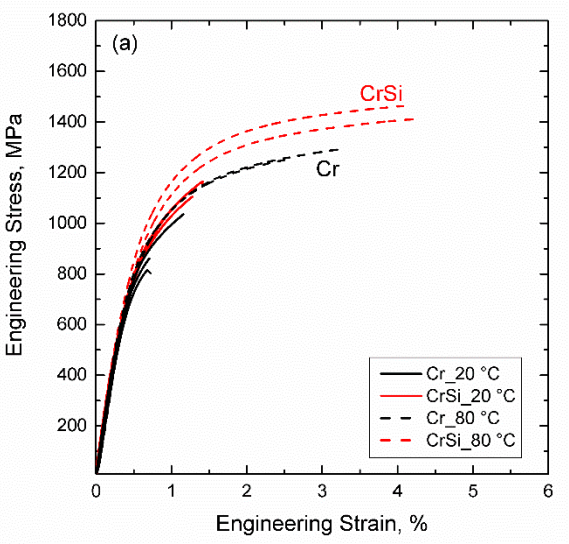


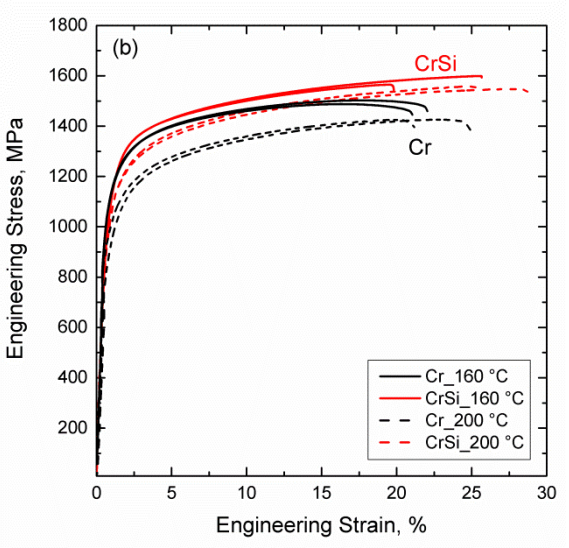


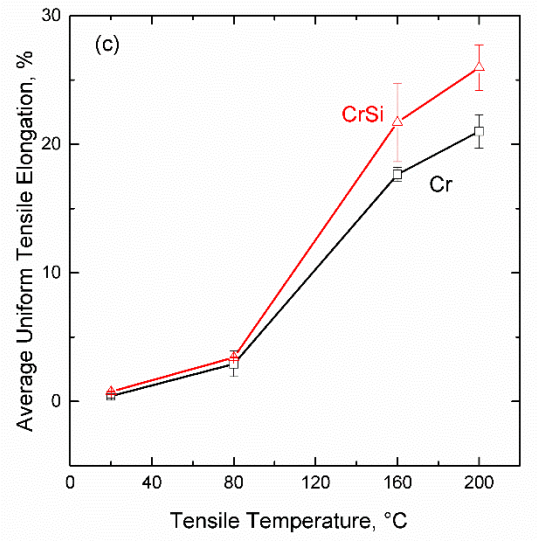


**Figure 5.** (a, b) Temperature dependence of engineering stress-strain curves for the steels treated by simplified Q&P processing according to Figure 1(b); (c) temperature dependence of uniform tensile elongation.

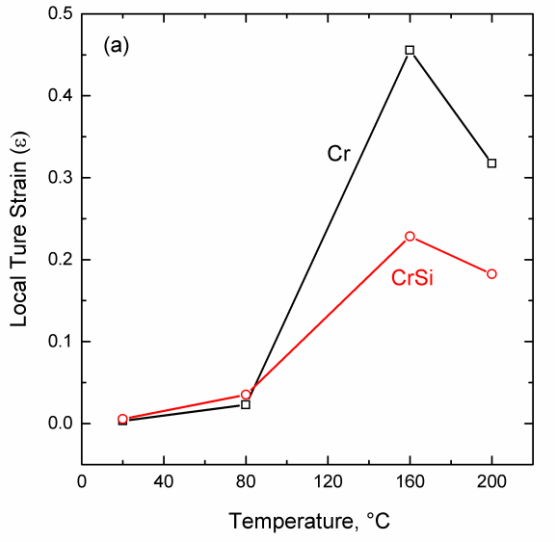


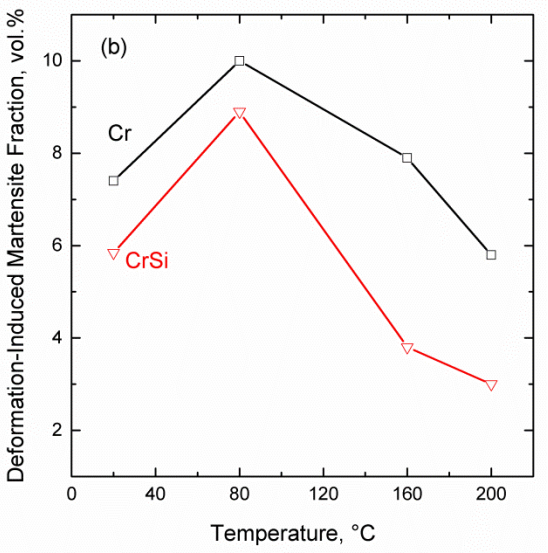

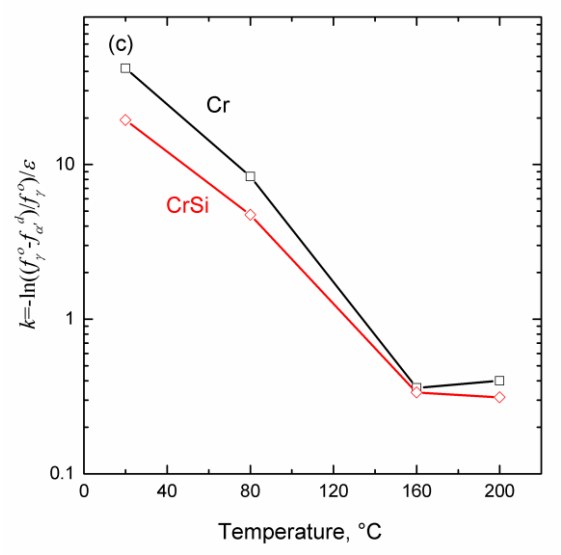


**Figure 6.** (a) Local true strains of the specimens taken from the gauge sections; (b) deformation-induced martensite fractions calculated from the martensite fractions of the specimens taken from the grip and the gauge sections of deformed tensile specimens; (c) Stability parameter $k$ at various tensile test temperatures calculated using equation (1) and the values in (a) and (b).

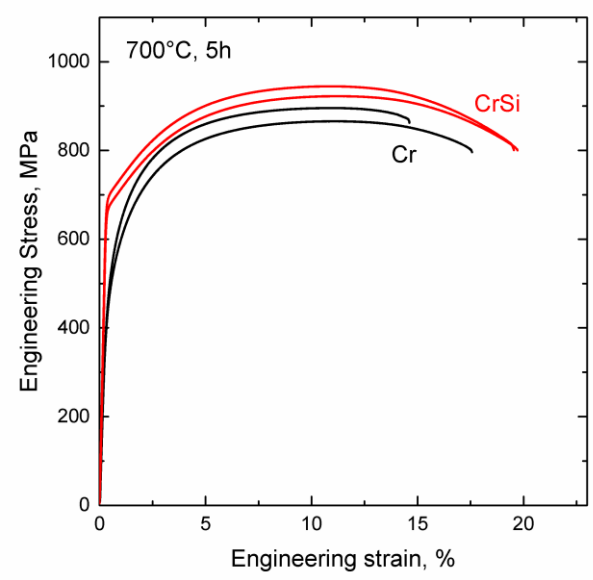


**Figure 7**. Flow curves of the steels soft-annealed at 700 °C for 5 h subsequent to Q&P processing according to Figure 1(b).

## 4. Conclusions

The influence of Si addition on the carbon partitioning during Q&P processing of stainless steels was investigated by the addition of 2 mass-% Si to the Fe-13Cr-0.47C steel. Q&P processing involving solution annealing at 1050 °C, quenching to various temperatures below $M_s$ temperature, and partitioning at 450 °C was performed in a dilatometer to evaluate the influence of Si on the thermal stability of austenite. A simplified Q&P processing involving solution annealing at 1250 °C, quenching to RT, and partitioning at 450 °C, on the other hand, was applied to tensile test specimens. The mechanical stability of RA was subsequently evaluated by tensile testing at temperatures between RT and 200 °C. The following conclusions were drawn:

1. According to dilatometry results, the carbon enrichment of austenite in the partitioning step was comparable for both steels.
2. Tensile specimens of Si-added and Si-free steels have nearly equal martensite fractions after the application of simplified Q&P. The difference in the mechanical stability of steels was negligible.

3. Since martensite in the Si-added steel was confirmed to be free of $M_3C$ cementite after partitioning, the importance of cementite suppression by Si addition on the efficiency of carbon partitioning might have been overestimated.
4. The higher tensile strengths of the Q&P processed specimens of the Si-added steel can be justified by the solid solution strengthening effect of Si.

## 5. References

[1] Clarke A J, Speer J G, Matlock D K, Rizzo F C, Edmonds D V and Santofimia M J 2009 Influence of carbon partitioning kinetics on final austenite fraction during quenching and partitioning *Scr. Mater.* **61** 149–52
[2] De Knijf D, Puype A, Föjer C and Petrov R 2015 The influence of ultra-fast annealing prior to quenching and partitioning on the microstructure and mechanical properties *Mater. Sci. Eng. A* **627** 182–90
[3] Gouné M, Danoix F, Allain S and Bouaziz O 2013 Unambiguous carbon partitioning from martensite to austenite in Fe–C–Ni alloys during quenching and partitioning *Scr. Mater.* **68** 1004–7
[4] Wendler M, Ullrich C, Hauser M, Krüger L, Volkova O, Weiß A and Mola J 2017 Quenching and partitioning (Q&P) processing of fully austenitic stainless steels *Acta Mater.* **133** 346–55
[5] Huang Q, Schröder C, Biermann H, Volkova O and Mola J 2016 Influence of Martensite Fraction on Tensile Properties of Quenched and Partitioned (Q&P) Martensitic Stainless Steels *Steel Res. Int.* **87** 1082–94
[6] Speer J G, Rizzo Assunção F C, Matlock D K and Edmonds D V 2005 The "quenching and partitioning" process: Background and recent progress *Mater. Res.* **8** 417–23
[7] Cooman B C D, Lee S J, Shin S, Seo E J and Speer J G 2016 Combined Intercritical Annealing and Q&P Processing of Medium Mn Steel *Metall. Mater. Trans. A* **48** 39–45
[8] Findley K O, Hidalgo J, Huizenga R M and Santofimia M J 2017 Controlling the work hardening of martensite to increase the strength/ductility balance in quenched and partitioned steels *Mater. Des.* **117** 248–56
[9] Ding R, Tang D, Zhao A, Dong R, Cheng J and Meng X 2014 Effect of intercritical temperature on quenching and partitioning steels originated from martensitic pre-microstructure *J. Mater. Res.* **29** 2525–2533
[10] Mola J, Luan G, Brochnow D, Volkova O and Wu J 2017 Tempering of Martensite and Subsequent Redistribution of Cr, Mn, Ni, Mo, and Si Between Cementite and Martensite Studied by Magnetic Measurements *Metall. Mater. Trans. A* 1–8
[11] Toji Y, Miyamoto G and Raabe D 2015 Carbon partitioning during quenching and partitioning heat treatment accompanied by carbide precipitation *Acta Mater.* **86** 137–47
[12] Caballero F G, Allain S, Cornide J, Puerta Velásquez J D, Garcia-Mateo C and Miller M K 2013 Design of cold rolled and continuous annealed carbide-free bainitic steels for automotive application *Mater. Des.* **49** 667–80
[13] Samanta S, Das S, Chakrabarti D, Samajdar I, Singh S B and Haldar A 2013 Development of Multiphase Microstructure with Bainite, Martensite, and Retained Austenite in a Co-Containing Steel Through Quenching and Partitioning (Q&P) Treatment *Metall. Mater. Trans. A* **44** 5653–64
[14] Kim B, Sietsma J and Santofimia M J 2017 The role of silicon in carbon partitioning processes in martensite/austenite microstructures *Mater. Des.* **127** 336–45
[15] Linke B M, Gerber T, Hatscher A, Salvatori I, Aranguren I and Arribas M 2017 Impact of Si on Microstructure and Mechanical Properties of 22MnB5 Hot Stamping Steel Treated by Quenching & Partitioning (Q&P)
[16] Toji Y, Matsuda H and Raabe D 2016 Effect of Si on the acceleration of bainite transformation by pre-existing martensite *Acta Mater.* **116** 250–62
[17] Luo Q, Kitchen M and Abubakri S 2017 Effect of Austempering Time on the Microstructure and Carbon Partitioning of Ultrahigh Strength Steel 56NiCrMoV7 *Metals* **7** 258

[18] Gui X, Gao G, Guo H, Zhao F, Tan Z and Bai B 2017 Effect of bainitic transformation during BQ&P process on the mechanical properties in an ultrahigh strength Mn-Si-Cr-C steel *Mater. Sci. Eng. A* **684** 598–605
[19] Huang Y, Li Q, Huang X and Huang W 2016 Effect of bainitic isothermal transformation plus Q&P process on the microstructure and mechanical properties of 0.2C bainitic steel *Mater. Sci. Eng. A* **678** 339–46
[20] Santofimia M J, Zhao L and Sietsma J 2009 Microstructural Evolution of a Low-Carbon Steel during Application of Quenching and Partitioning Heat Treatments after Partial Austenitization *Metall. Mater. Trans. A* **40** 46–57
[21] Babu S S, Specht E D, David S A, Karapetrova E, Zschack P, Peet M and Bhadeshia H K D H 2005 In-situ observations of lattice parameter fluctuations in austenite and transformation to bainite *Metall. Mater. Trans. A* **36** 3281–9
[22] Ghazvinloo H R, Honarbakhsh-Raouf A and Rashid A R K 2015 Mechanical Properties of a High Si and Mn Steel Heat Treated by One-Step Quenching and Partitioning *Metallurgist* **59** 90–6
[23] Tsuchiyama T, Tobata J, Tao T, Nakada N and Takaki S 2012 Quenching and partitioning treatment of a low-carbon martensitic stainless steel *Mater. Sci. Eng. A* **532** 585–92
[24] Mola J and Cooman B C D 2013 Quenching and Partitioning (Q&P) Processing of Martensitic Stainless Steels *Metall. Mater. Trans. A* **44** 946–67
[25] Mesquita R A and Kestenbach H J 2011 M3C and M7C3 Carbide Precipitation in Modified H11 Tool Steel *Solid State Phenom.* **172**–**174** 414–9
[26] Tobata J, Ngo-Huynh K-L, Nakada N, Tsuchiyama T and Takaki S 2012 Role of silicon in quenching and partitioning treatment of low-carbon martensitic stainless steel *ISIJ Int.* **52** 1377–1382
[27] Huang Q, Cooman B C D, Biermann H and Mola J 2016 Influence of Martensite Fraction on the Stabilization of Austenite in Austenitic–Martensitic Stainless Steels *Metall. Mater. Trans. A* **47** 1947–59
[28] Huang Q, Volkova O, Biermann H and Mola J 2017 Dilatometry Analysis of Dissolution of Cr-Rich Carbides in Martensitic Stainless Steels *Metall. Mater. Trans. A* **48** 5771–7
[29] Huyan F, Larker R, Rubin P and Hedström P 2014 Effect of Solute Silicon on the Lattice Parameter of Ferrite in Ductile Irons *ISIJ Int.* **54** 248–50
[30] Huang Q, Volkova O, Biermann H and Mola J 2017 Tensile elongation of lean-alloy austenitic stainless steels: transformation-induced plasticity versus planar glide *Mater. Sci. Technol.* **33** 1224–30
[31] Mola J, Ullrich C, Kuang B, Rahimi R, Huang Q, Rafaja D and Ritzenhoff R 2017 Austenitic Nickel- and Manganese-Free Fe-15Cr-1Mo-0.4N-0.3C Steel: Tensile Behavior and Deformation-Induced Processes between 298 K and 503 K (25 °C and 230 °C) *Metall. Mater. Trans. A* **48** 1033–52
[32] Sugimoto K-I, Kobayashi M and Hashimoto S I 1992 Ductility and strain-induced transformation in a high-strength transformation-induced plasticity-aided dual-phase steel *Metall. Trans. Phys. Metall. Mater. Sci.* **23 A** 3085–91

**Acknowledgments**
The financial support of German Research Foundation (DFG) under grant number MO 2580/1–1 is gratefully acknowledged. Authors extend their thanks to the technical staff at the Institute of Iron and Steel Technology of TU Bergakademie Freiberg for their assistance.